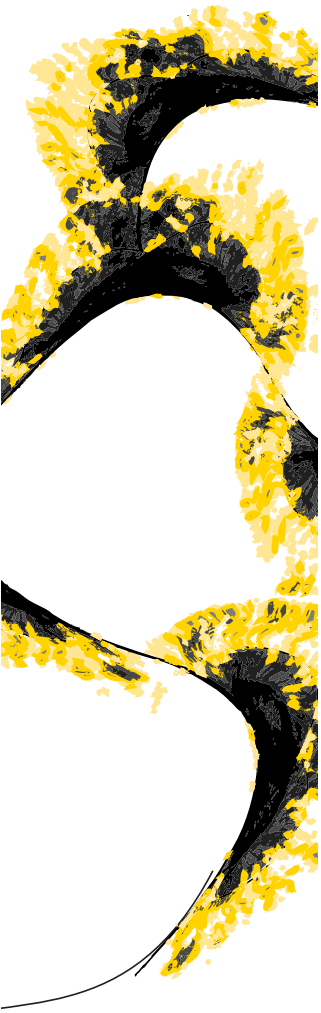

RAM ROBOTICS AND MECHATRONICS

MOTION CONTROL OF A HELICAL UNTETHERED MAGNETIC ROBOT WITH A ROTATING PERMANENT MAGNET FOR MINIMALLY INVASIVE NAVIGATION OF COMPLEX VASCULAR STRUCTURES

P. (Pelin) Akca

BSC ASSIGNMENT

Committee:
dr. I.S.M. Khalil
dr. G. Dagnino
dr. J. Dasdemir

February, 2025

006RaM2025
Robotics and Mechatronics
EEMCS
University of Twente
P.O. Box 217
7500 AE Enschede
The Netherlands

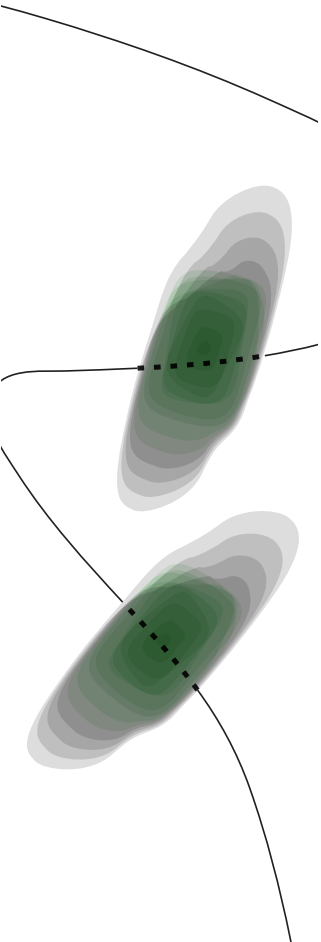

UNIVERSITY OF TWENTE. | TECHMED CENTRE UNIVERSITY OF TWENTE. | DIGITAL SOCIETY INSTITUTE

Abstract

Advancements in minimally invasive surgical microrobots have provided opportunities to explore complex vascular structures within the cerebral vasculature. Examples of multiple trajectories will be demonstrated during this study. The pathway beginning from the Common Carotid Artery towards the Internal Carotid Artery or External Carotid Artery will be explored using a helically shaped Untethered Magnetic Robot (UMR). Additionally, the pathway to reach an aneurysm within the phantom will be explored, and a procedure to navigate multiple UMRs to this location to induce coagulation will be explained. The motion control of this helical UMR will be achieved through the use of a Rotating Permanent Magnet, which generates a magnetic field to guide the microrobot. The challenge is to guide the microrobot through a tortuous environment with varying narrow diameters. It is beneficial to know the frequency range in which the UMR reaches a controlled maximum propulsion speed. The frequency of the permanent magnet directly influences the performance of the UMR, providing knowledge on the velocities the UMR can reach. The trials were successful, since the UMRs we able to navigate through the trajectories and back when needed. These findings will result in a better understanding of motion control in complex vascular environments and therefore enhance insights into minimally invasive procedures with reduced recovery time and patient trauma. A next step would suggest to explore the cerebral vasculature further, as this UMR has the potential to navigate the entire system.

1 Introduction

The cerebral vasculature is an intricate system which supplies the brain with all its metabolic and neurological demands, which involves its sensitivity to hypoxia and toxicity, maintenance of functions such as homeostasis, autoregulation of blood flow and facilitating neurovascular coupling. Ideally, critical conditions such as strokes and brain aneurysms would be treated with minimal invasion and patient trauma, without compromising properties as safety and precision. Additionally, blood clots or other types of embolisms in arterial regions that are small in diameter or have a tortuous nature can be challenging to access with traditional tethered approaches. These conditions can instead be treated effectively using the approach regarding this ongoing research, by using Untethered Magnetic Robots (UMRs) within the cerebral vascular system as a minimally invasive solution. These UMRs are guided by an external magnetic field created by a Rotating Permanent Magnet (RPM), to enable precise medical procedures within complex vascular structures.

In previous trials [1] the Common Carotid Artery (CCA) was used as an entry point, and from there the External Carotid Artery (ECA) and the Internal Carotid Artery (ICA) were successfully explored using a phantom mimicking the cerebral vascular system, which can be viewed in figure 1. Now, a next step would be to extend this pathway using a UMR of a smaller diameter, to be able to navigate the entire cerebral vascular system. To clarify, the ECA and ICA have a diameter of approximately 4 - 4.3 mm and 4.3 - 5.8 mm. The navigation of these blood vessels should first be done successfully, before moving onto further paths. To extend to the Anterior Cerebral Artery (ACA), Posterior Cerebral Artery (PCA) and Middle Cerebral Artery (MCA), which are the results of the branching of the ICA, a UMR with a diameter < 2 mm is required. The reason for this is due to the diameters of the ACA, PCA and MCA which are approximately 2.8 mm, 2 - 3 mm and 3 - 5 mm. Therefore, a UMR with a diameter of 1.5 mm will be used, since this ensures that the UMR can circulate fully around its z-axis with minimal chance of touching the inner lining of the vessel.
Nelson *et al.* have introduced a helical magnetic continuum robot, which navigates with the use of an external magnetic field. The magnetic field is generated using stationary electromagnets, and the robot is applied to navigate dense and tortuous blood vessels of the brain [2]. Similarly, Becker *et al.* introduced their helical miniature magnetic swimmer, which navigates a 3D space using a permanent rotating magnet. The focus was on the removal of blood clots and was achieved using closed loop motion control[3].

1.1 Aneurysm Inside Cerebral Vascular Phantom

The cerebral vascular phantom contains a well-defined aneurysm, which resemble the most common type of aneurysms: a succular intercranial aneurysm. These have a perfect round dome and neck, and are usually found near bifurcations of the ACA, MCA or PCA. This description fits the description of the aneurysm found on the phantom, since its location is on the Anterior Communicating Artery, which connects the left and right Anterior Cerebral Artery [4]. A common suitable method to remove this type of aneurysm, is by applying surgical clipping. After performing a craniotomy, the blood supply to the aneurysm is cut off using one or multiple clips while still maintaining the blood supply to the parent vessel. Another method is endovascular coiling, where a microcatheter is navigated into the aneurysm with the assistance of microguidewires. Detachable coils pack the volume of the aneurysm and induce blood clot formation [5]. Coiling comes with the potential of complications during the procedure. The most common complications are tromboembolic com-

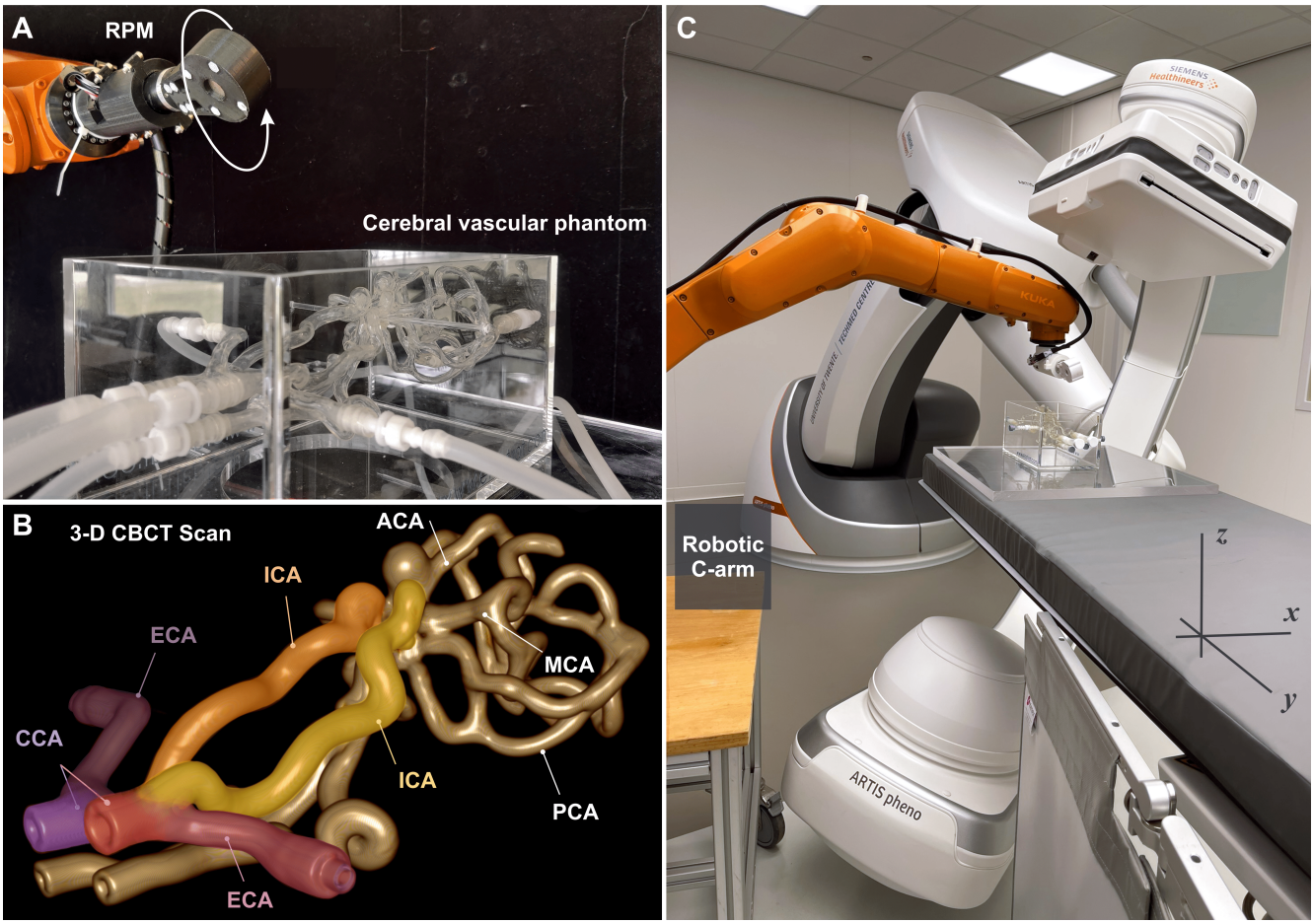

Figure 1: Overall images of the complete setup using the cerebral vascular phantom. A) Here the Rotating Permanent Magnet is shown together with the phantom and an example of the gap between these two can be observed. B) Here a 3D model of the phantom is shown, with the branches from the right and left CCA. The ECA and ICA will be explored in this study. The aneurysm between the ICA and ACA can also be seen. C) Here a setup is shown with a CBCT scanner to gather data from all possible perspectives.

plications, which is an umbrella for a variety of complications. Common occurrences are that a clot is formed at the neck of the aneurysm caused from the coiling, which could cause occlusion in the parent vessel or migration to a further vessel. When there is an occlusion in the parent vessel, it could also be caused by the microcatheter damaging the inner lining of the vessel. This could trigger clot formation or could make the vessel spasm, which results in narrowing. These complications are difficult to treat, since giving the patient antiplatelet medication could result in rupture of the aneurysm. To open the vessel and continue the coiling procedure, a balloon or stent needs to be inserted. Another complication is coil migration, which could vary from a small displacement near the aneurysm neck to complete displacement from the aneurysm. This could then result in tromboembolic complications due to clot formation around the migrated coil. Lastly, there is the complication that the aneurysm could rupture during the procedure. Perforation of the aneurysm can be caused by either the microguidewire or the microcatheter [6].

1.2 Motion Control of Untethered Magnetic Robot

The motion control of the UMR is done with the use of a permanent magnet. The permanent magnet creates a magnetic field which enables the UMR to move in a forward and backward direction, depending on the direction of the magnetic field. Here, the rotation axis of the permanent magnet has a parallel alignment with the vessel of the cerebral phantom, to ensure the UMR swims in this direction. This ability to move in a forward and backward direction can be applied in a tortuous environment. The UMR consists of a magnetic core enabling the swimming response to the magnetic field. In combination with the helical shape, the UMR propels through fluid and could potentially be applied for various medical procedures. The response to the

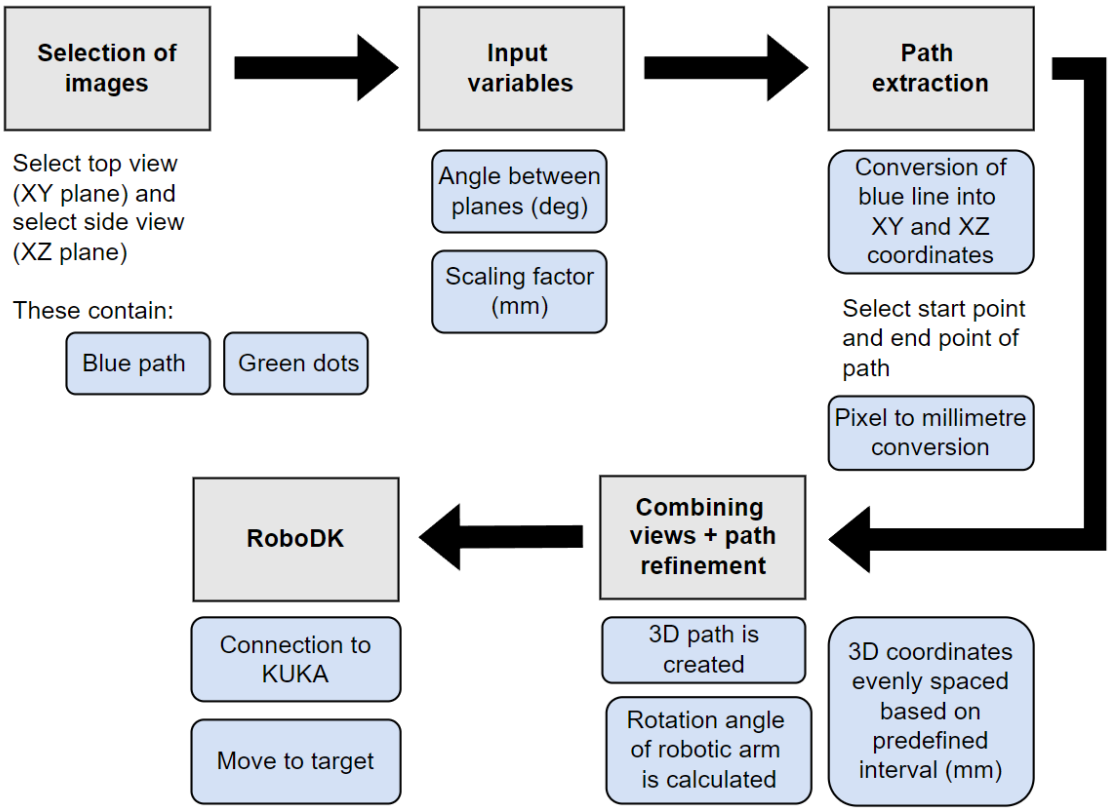

Figure 2: Diagram of the open-loop motion control of the Untethered Magnetic Robot

external magnetic field is dependent on the ferromagnetic material that creates the magnetic core. This also determines the magnetic moment, directly affecting the magnetic torque and the controlled navigation. Increasing the amount of material within the core would therefore also increase the magnetic torque but would at the same time add mass to the UMR, influencing its navigating abilities [7]. Added mass could potentially result in the UMR sinking within the fluid due to increased gravitational force. It is for this reason that a balance needs to be determined in the distance between the UMR and the RPM. With this RPM-UMR gap, there is an ideal distance that creates balance between magnetic and gravitational forces. Another benefit of optimizing this gap is that the UMR would be dragged upwards by the magnetic field, when the distance would be too short. This would cause the swimming behaviour to disappear and as a result the UMR would not be controlled any more, since it would strictly swim toward upper branches[1].

In figure 2 a diagram of the open-loop 3D control is shown. To have the robotic arm follow the correct trajectory, several steps need to be taken. It begins with inserting images that represent an anterior view (XY plane) and a lateral view (XZ plane) of the blood vessels the UMR needs to navigate through. These images need to contain 2 factors: 1) a blue line (RGB = 0,0,255) representing the path and 2) two separate green dots (RGB = 0,255,0) representing a known distance to convert pixels to millimetres. To provide more information, the angle between the planes (most likely 90 degrees) and the distance between the green dots (in mm) are used as input variables. From this information, a new trajectory (in red) is presented, and the user is asked to select the start and end points. Now the XY-coordinates, XZ-coordinates, the conversion from pixel value to millimetres and the start and end points are known. The 3D path can be derived, by mapping the coordinates of the XY plane and the XZ plane. The spacing of the 3D coordinates is based on the predefined interval value (mm). This means that a low interval value could be beneficial, when a physical path contains many details. However, when this is not the case a low interval value could result in unnecessary steps which are time-consuming. The angle of the RPM is also determined. This information is passed on to RoboDK [8] where the coordinates are treated as targets, to which the end-effector of the robotic arm has to move.

1.3 Physiology Cerebral Vasculature

Information on the anatomy and physiology of the blood vessel will clear up some of the obtained results.

Arteries including the aorta and its branches are considered elastic arteries, and are characterized by being thick-walled. They range in diameter from 10 mm - 25 mm and are low-resistance and therefore the most elastic. As the heart pumps, these arteries expand and recoil and therefore have a pressure smoothing ability. These elastic arteries give a way to the muscular arteries, that range from 6 mm down to 0.3 mm, which is more consistent with the diameter seen in the cerebral vascular phantom. These arteries have the thickest tunica media layer of all vessels, which has the responsibility of maintaining blood flow and pressure. Depending on the demand, the cells in this layer can increase or decrease the diameter of the vessel. Small fluctuations in diameter has a great influence on the blood flow and pressure, meaning that in in vivo environments these are factors that need to be taken into account [4].

2 Results of Motion Control

2.1 Frequency Response of Untethered Magnetic Robot

As a first step, a straight tube of a diameter of 3/16 inch (4.8 mm) was used. The purpose of this experiment was to determine the frequency response of the UMR. Here, frequencies up to the maximum capability of the RPM, which is equal to 40 Hz, were applied with a gap of 150 mm between the RPM and the UMR. The velocity at the specified frequency was measured, which was done using 3 UMRs of which one did not have a coating to enhance the biocompatibility in an in vivo environment. The remaining two UMRs did have this coating.

The results of all 3 UMRs can be viewed in figure 3a. The expectations of the results were to see a linear increase in velocity when the frequency was increased in steps of 2 Hz. The actuation frequency of 40 Hz is the value that the RPM cannot exceed, meaning if the linear behaviour continues at 40 Hz the step-out frequency of the UMR is not yet reached at this point. The timeline in this process was that first an uncoated UMR was tested, and then a coated UMR. Based on the obtained response, a third UMR with the coating was tested again to confirm the linearity that was observed. In the responses of the 3 UMRs in figure 3a it can be clearly observed that the coated UMRs reach a higher velocity over the whole frequency range, compared to the uncoated UMR. The coated UMRs also seem to be more linear compared to the uncoated UMR, which shows a direct relation with the obtained results and the expectations. From this visualization, the linearity of the coated UMRs seems to be fitting the expectations better compared to the uncoated UMR. To confirm these observations, the R^2 values were determined. The coefficient of determination, also known as the R^2 value, determines the proportion of the variance of how much the dependent variable is predictable from the independent variable in the model. Here, the independent variable is the frequency and the dependent variable is velocity of the UMR as a response to the magnetic field. An R^2 value of 1 is the largest possible value, and the closer the value is to this the more variability is explained by the model. The R^2 value can be obtained using the MATLAB function *fitlm* [9], which results in:

$$R^2 = 1 - \frac{\sum_{i=1}^{N}(y_i - \hat{y}_i)^2}{\sum_{i=1}^{N}(y_i - \bar{y})^2}. \tag{1}$$

Here, N represents the total number of data points, y_i the measured values, $\hat{y}_i$ the predicted values, and $\bar{y}_i$ the mean of the measured data [10]. Here the following results were obtained: UMR1 (uncoated): 0.907; UMR2 (coated): 0.954; UMR3 (coated): 0.965. The obtained R^2 values are all close to 1, meaning that all three models are a relatively good fit. However, UMR2 and 3 indicate approximately 95.4% and 96.5% of the variance, compared to only 90.7% of the UMR1, meaning that the coated UMRs align better with the expected results and therefore it would be ideal to work with coated UMRs.

The effect of boundaries of the magnetic field can be visualized very clearly in the results. In the lower frequency range, between 12 and 16 Hz, there is not a large increase in velocity because the UMR loses its horizontal orientation rapidly due to the curvature of the magnetic field resulting from the RPM. Once the frequency increases, the horizontal pathway increases as well, meaning the UMR can hold its maximum velocity for a longer time. This way, the average velocity of the pathway in one direction increases as the frequency increases. In the frequency range between 36 and 40 Hz there is a clear divergence in the results, where the coated UMRs seem to have a jump in their velocities compared to the uncoated UMR, which has a decline. Interesting at this higher frequency range is that the standard deviations in figure 3b have a sudden jump as well. The standard deviations over the course of the entire frequency range seem to be relatively low and consistent, until a value of approximately 32 Hz is reached, where the standard deviations only increase. This indicates an increase in inconsistent responses and therefore make the behaviour of the UMR more unpredictable.

2.2 Hemocompatible Lipid Coating

As mentioned above, a coating was applied to the UMRs. This lipid-based coating has the purpose of ensuring hemocompatibility of the UMR when inserted into the bloodstream. In prior research, the coating has shown promising results regarding cell adhesion, morphology, proliferation, and differentiation, with the ad-

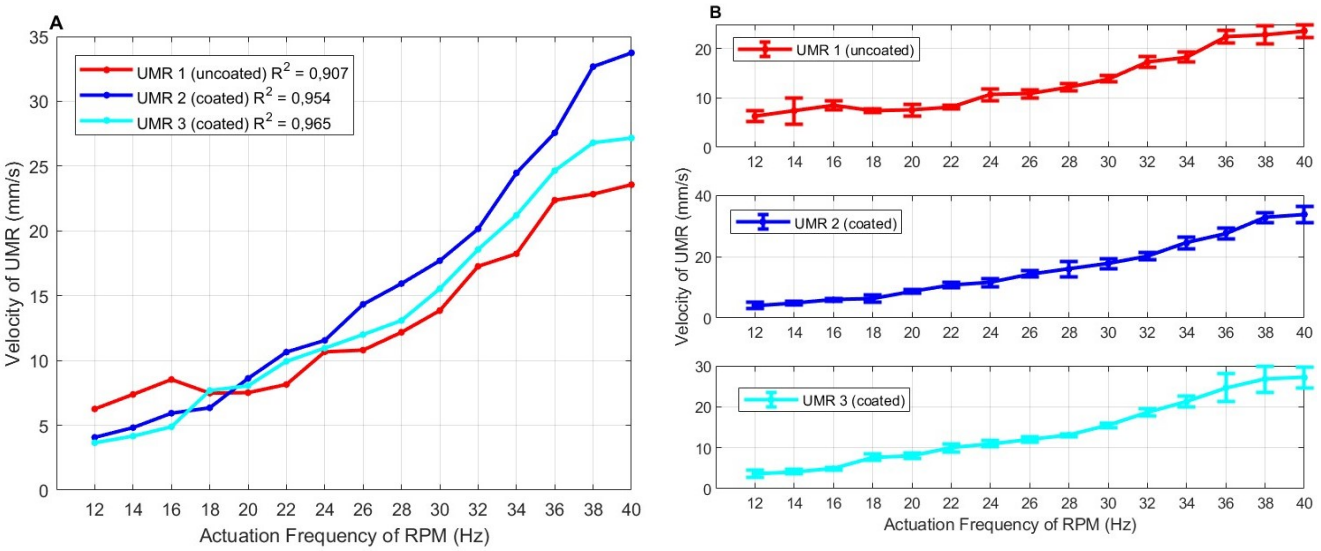

(a) Frequency response of 1.5 mm UMRs determined in an 3/16 inch (4.8 mm) straight tube.

(b) Results from the frequency response plotted separately and with the addition of the standard deviation.

Figure 3: Results from the frequency response test using 3 UMRs. Here, each UMR swam 3 times forward and backward over the trajectory and the average of these values was taken.

dition of focal adhesion formation [11]. In additional prior research, various tests were carried out to ensure the hemocompatibility [12]. In vivo factors such as protein fouling, biofilm formation and other hemocompatibility assays were investigated. After incubation with fluorescently labelled fibrinogen, the UMR material showed a 95% reduction in fibrinogen adsorption on the coated samples compared to the uncoated ones. The lack of affinity of fibrinogen towards the UMR material gives an indication of the hemocompatibility, and this reduction of protein fouling will reduce the activation of clotting and the complement system during in vivo experiments. Furthermore, there was a reduction of more than 99% of formed biofilms resulting from bacterial infections on the coated samples, meaning that the coated UMRs have a reduced risk of causing infection. Lastly, when the formation of blood clots was investigated, fibrin generation was compared using platelet poor plasma. The fibrin generation was delayed by > 6 minutes for the coated compared to uncoated samples. From these assays the conclusion can be drawn that coated UMRs will be highly hemocompatible during in vivo applications.

From prior research mentioned above [12] it can be determined that the surface roughness of the lipid-coated UMR is reduced, considering the reduction in protein fouling by 95% and the reduction of the biofilm formation of $> 99\%$. This ensures a smoother surface which leads to minimized resistance during locomotion. Also the delay in fibrin generation (> 6 minutes) reduces the formation of clots around the UMR, which would otherwise increase viscous drag. The reduction in surface roughness and viscous drag is between the surface of the UMR and the surrounding fluid, which in the conditions of these results was blood. In the conditions of the obtained frequency response shown in figures 3a and 3b tap water was used, meaning the findings found above are not applicable. The lipid base does however causes a hydrophobic layer on the UMR. This reduces water adhesion on the surface of the UMR, still minimizing drag in the fluid. Drag force can be described by:

$$F_D = \frac{1}{2}\rho v^2 C_D A \ , \tag{2}$$

where F_D is the drag force (N), ρ the fluid density (kg/m^3), v velocity of the object (m/s), C_D the drag coefficient and lastly A the cross-sectional area of the object (m^2). Here the drag coefficient is dependent on the shape of the moving object in the fluid and the smoothness of the surface. The difference between the coated and uncoated UMRs in water is the smoothness created by the lipid-based layer. The results in figure 3a show that the coated UMRs are able to reach higher velocities, which can be verified by the fact that they have a smoother surface and therefore are less affected by drag. The smoothness of the surface can also be a direct explanation to the predicable behaviour of the coated UMRs. The shear stress at the wall of the blood vessel is reduced due to the reduced drag. The shear stress can be described by:

$$\tau_w = \mu \left(\frac{\partial u}{\partial y} \right)_{y=0} \ , \tag{3}$$

where: τ_w is the wall shear stress (Pa), μ the dynamic viscosity (Pa $\cdot$ s) and $\frac{\partial u}{\partial y}$ the velocity gradient (s^{-1}). To determine the total shear force (N) on the wall of the blood vessel, the shear stress can be multiplied with the area. The reduced F_D means that the coated UMRs are swimming with less resistance, which affects the velocity profile $\frac{\partial u}{\partial y}$ of the fluid inside the vessel. Reduced $\frac{\partial u}{\partial y}$ implies in this case that the UMR is swimming with an increased constant velocity. This can be verified by the lower R^2 value of the uncoated UMR, indicating more fluctuations in the velocity profile. In 1.3 it was explained how the change in pressure and flow can be accounted for by the blood vessel, meaning that changes in the velocity profile are as little desired as possible. This is because changes caused by the UMR will then change the diameter of the vessel and therefore could potentially cause more turbulent flow [13].

2.3 Performance of Motion Control Inside Cerebral Vascular Phantom

After determining the frequency response of the 1.5 mm UMR, the phantom mimicking the cerebral vasculature was used in various trails. Here, different paths were tested, which can all be viewed in figure 4, and the velocities can be viewed in table 1. Only uncoated UMRs were used, as they were the only type available at the time of the study. For all trials, the RPM-UMR gap was again equal to 150 mm, to match with the results from the frequency response. The lowest z-value was set to 85 mm, meaning the RPM would not exceed this gap to insure the safety of the trial. All trials were done twice ($n = 2$), and it is important to note that all trials were recorded from a posterior view.

Right CCA to right ECA

This vascular route starts at the proximal end of the right CCA and continues until the distal end of the right ECA. When the bifurcation is reached by the UMR, the RPM-UMR gap decreases to attract the UMR and prevent it from going into the right ICA. At the distal end of the right ECA, the RPM direction is inverted and the UMR moves in the backward direction over the equivalent path. An actuation frequency of 24 Hz was used and with this the value for the forward average velocity is equal to 8.2 $\pm$ 0.42 mm/s and the backward average velocity is 15.4 $\pm$ 0.99 mm/s ($n = 2$).

Right CCA to right ICA

Now, for the right CCA to the right ICA the path length increases, compared to the right ECA pathway. Here the UMR falls into the bifurcation due to gravitational force. Throughout the route the RPM-UMR gap decreases when the UMR needs to move against gravity. At the distal end of the right ICA the RPM inverts its direction and the UMR follows the equivalent path into the backward direction. The actuation frequency that was used here was 24 Hz, and it resulted in a forward average velocity of 6.2 $\pm$ 0.99 mm/s and a backward average velocity of 21.2 $\pm$ 6.4 mm/s

Left CCA to left ECA

On the left side of the phantom the UMR moves from the proximal end of the left CCA to the distal end of the left ECA. At this bifurcation, the UMR will more easily swim into the left ECA due to gravitational force, unlike the right ECA. Here it again follows the route until the distal end of the vessel, and returns at the equivalent path. The actuation frequency here was again 24 Hz, and the forward average velocity equals to 11.4 $\pm$ 4.2 mm/s and the backward average velocity equals to 10.8 $\pm$ 3.2 mm/s ($n = 2$).

Left CCA to left ICA

Lastly, there is the path from the proximal end of the left CCA to the distal end of the left ICA. Here the bifurcation begins with a steep upwards path, and continues with a steep downwards path and is followed by a horizontal path and then has a steep increase again. Due to the complexity of this bifurcation, an actuation frequency of 26 Hz was needed. This resulted in a forward average velocity of 6.2 $\pm$ 0.07 mm/s and a backward average velocity of 17.2 $\pm$ 3.0 mm/s ($n = 2$).

2.4 Aneurysm Inside Cerebral Vascular Phantom

In 1.1 the aneurysm in the phantom was briefly mentioned. Here different procedures were explained on how to treat an aneurysm, one of which was endovascular coiling. A trial was done where the UMR was navigated towards the aneurysm, to mimic the coiling procedure. The idea here is that a group of UMRs navigate one by one to an aneurysm and stimulate coagulation. In this case, 2 UMRs were navigated to the aneurysm. A path starting from the proximal end of the left CCA, continuing on the left ICA and reaching the aneurysm was explored using the 1.5 mm UMRs at an actuation frequency of 26 Hz. The RPM-UMR gap was equal to 150 mm and the lowest z-value was set to 85 mm. Both UMRs that were used were coated and the trials were again recorded from a posterior view. In figure 5 the paths are shown and in table 2 the velocities (mm/s) of the first and second UMR can be viewed. To clarify, first UMR (UMR1) was navigated to the aneurysm with an average velocity of 4.3 mm/s. Important to note here is the difference in velocity before and after surpassing the distal end of the left ICA. The velocity from the left CCA to the left ICA is 7.4 mm/s, and the velocity from the left ICA to the aneurysm is 1.2 mm/s. The second UMR (UMR2) has an average total velocity of 5.0 mm/s. Before the end of the left ICA it has a velocity of 8.4 mm/s and after it has a velocity of 1.6 mm/s.

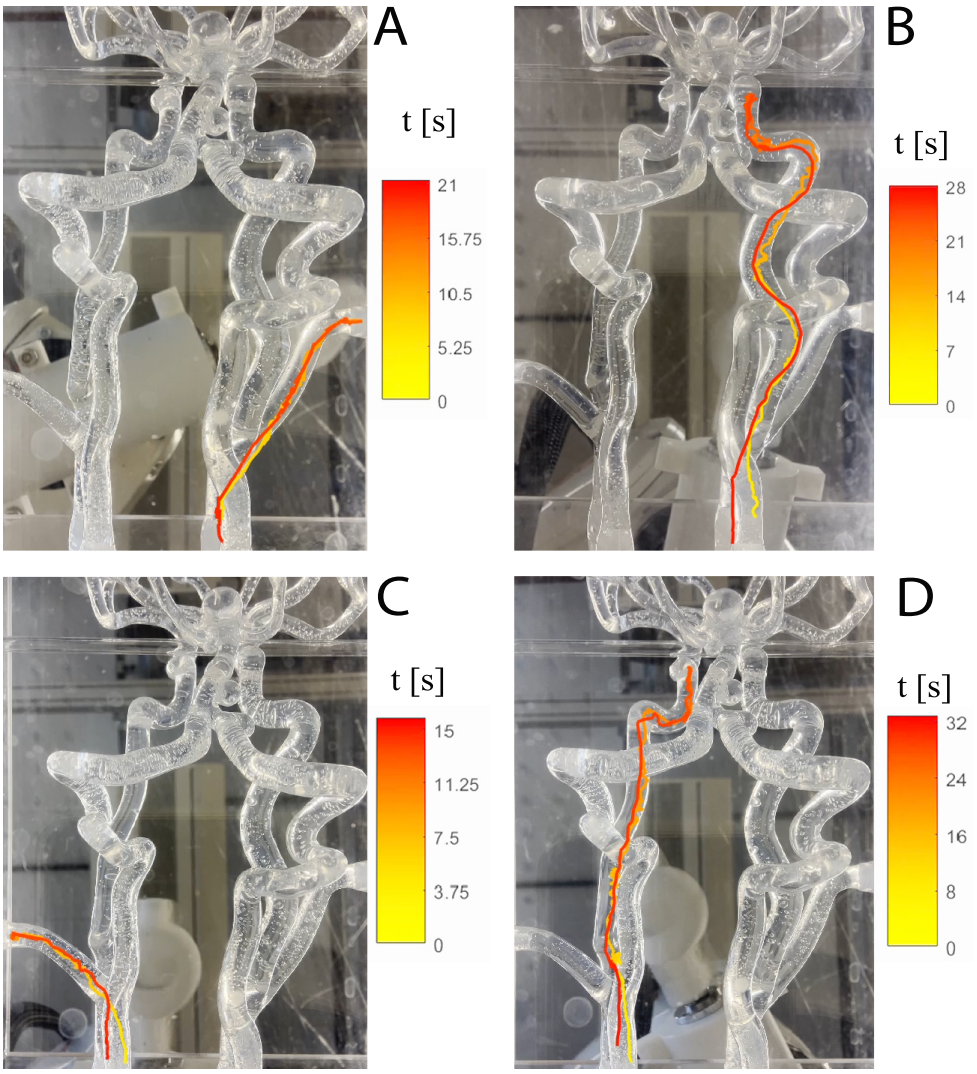

Figure 4: All 4 trajectories shown with the path the UMR surpassed. The colour from the path and from the colourbar indicates the time in seconds. A) from the right CCA to the right ECA, B) from the right CCA to the right ICA, C) from the left CCA to the left ECA and D) from the right CCA to the right ICA.

Table 1: The forward and backward average velocities from 4 trajectories ($n = 2$).

Route	**Forward average velocity [mm/s]**	**Backward average velocity [mm/s]**
Right CCA to right ECA	8.2 ± 0.42	15.4 ± 0.99
Right CCA to right ICA	6.2 ± 0.99	21.2 ± 6.4
Left CCA to left ECA	11.4 ± 4.2	10.8 ± 3.2
Left CCA to left ICA	6.2 ± 0.07	17.2 ± 3.0

2.5 Evaluation of experimental findings

The controlled navigation to the left and right ECA and ICA were successful. The further vessels could potentially be reached with the UMR of this diameter, since a diameter of 2 mm would already be sufficient to explore the entire cerebral vascular system. Overcoming complex bifurcations and other structures have been proven to be successful as well. Interesting to note is that the backward average velocity is notably higher than the forward average velocity. The difference here is the response of the motors of the RPM, which clearly work more efficiently when the direction of the magnetic field is towards the RPM, since this results in backwards swimming. Considering this finding, the angle of the RPM is a topic to be considered in future trials. A frequency range of 24 - 26 Hz was used, of which the average velocities match with the findings of the frequency response shown in figure 3a.

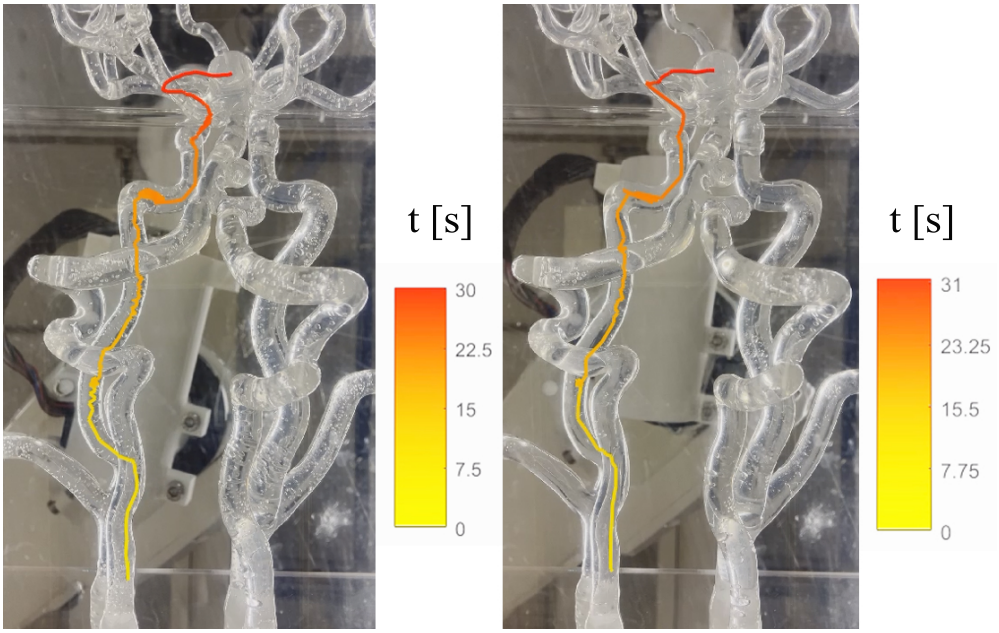

Figure 5: The trajectory from the left CCA to the aneurysm is shown twice. The colour from the path and from the colourbar indicates the time in seconds. A) the first UMR reaches the aneurysm and B) the first UMR maintains inside the aneurysm, while a second UMR reaches the same target.

Table 2: Forward average velocities of the trajectory of the left CCA to the left ICA and the aneurysm.

	Left CCA - ICA [mm/s]	**Left ICA - aneurysm [mm/s]**	**Total average velocity [mm/s]**
UMR1	7.4	1.2	4.3
UMR2	8.4	1.6	5.0
Average	7.9 ± 0.7	1.4 ± 0.3	4.7 ± 0.5

Important to note here is that the findings in figure 3a are an average of the forward and backward velocities, meaning the increased velocity found in the backward direction cannot be observed in that figure. The trials could possibly be done again, with this time a coated UMR and the outcomes could be compared to these results. Lastly, the number of trials is also a topic to be considered in the future. Currently, only 2 trials were done per path ($n = 2$) due to time restrictions, which could result in unreliable findings. Regarding the findings of the aneurysm, both UMRs successfully reached the target, which means that this could potentially be applied as a medical procedure. Issues such as coil migration could be reduced, considering that when there are 2 UMRs in this aneurysm the UMRs stick together due to magnetic attraction and their collective diameter becomes 3 mm. This is too large to leave the aneurysm, meaning migration is not likely to become a medical complication. The only situation in which it could become a complication, is when there is one UMR in the aneurysm and a second UMR is being navigated towards it. Here, the UMR in the aneurysm could potentially escape and swim in a connecting vessels. In 2.2 it was mentioned how the lipid coating has been proven to be hemocompatible, and therefore has a small likelihood of clot formation. Now, this is beneficial when the UMR is navigating through blood vessels; however, clotting is required if the goal is to treat the aneurysm by navigating a group of UMRs towards it. The results regarding the coating did not rule out clot formation, only that it was delayed. Further tests should be done to determine if this procedure should be done with or without the hemocompatible coating.

With motion control, the likelihood of the UMR damaging the inner lining of the parent vessel, or causing the rupture of the aneurysm could be reduced as well. This trial also gave the opportunity to compare the velocity of the uncoated and coated UMRs. In table 1 the forward average velocity of the left CCA to the left ICA can be found, which equals 6.2 ± 0.07 mm/s. In table 2 the (forward) average velocity of this path equals to 7.9 ± 0.7 mm/s. This supports the findings of the frequency response, where higher velocities for the coated UMRs were found as well.

2.6 Materials and Methods

Frequency Response
To obtain the results for the response of the UMR to the frequency range, the following procedure was applied. A straight tube phantom of 3/16 inch (4.8 mm) was filled with tap water and the UMR was inserted. The UMR was able to move using the RPM, which creates a magnetic field and attracts the UMR that has an inner magnet. The values of the UMR and the inner magnet can be viewed in table 3. The orientation of the RPM is managed by a KUKA 6-DOF manipulator (KUKA KR-10 1100-2, KUKA, Augsburg, Germany) and the rotational velocity is managed using a Maxon 18 V brushless DC motor. 2 screws were added to the setup and the distance in between was measured with the purpose of adding a scaling factor. Visualization was obtained using a webcam setup. The frequency range goes from 0 - 40 Hz, and in order to obtain the response steps of 2 Hz were used. At 12 Hz the UMR was able to swim for the first time, and from here on the UMR swam until it got stopped by the range of the magnetic field. The orientation of the RPM would switch at this point, and the UMR would swim in the opposite direction until it got stopped by the magnetic field again. This process was repeated 3 times per frequency and recorded by the webcam from a lateral view. These results were then imported into Tracker [14], which is an image recognition application. Here, the distance the UMR travelled against the time was determined, and with that information the velocity can be calculated. To do this calculation, a MATLAB script was used.

Control Inside the Phantom
The control inside the cerebral vascular phantom has similarities to the control used to obtain the frequency response. The phantom was again filled with tap water and the UMR was controlled with the KUKA robotic arm. However, here the path was determined beforehand using a path generating application from RoboDK Inc [8]. The various paths were tested and recorded using a camera setup which had an posterior view on the setup. Further processing of the data was done using Tracker and Matlab, where the average velocity and the visualization of the trajectory were determined.

Table 3: Properties of the UMR and the magnet in the core of the UMR.

Properties UMR & Magnet	**Value**	**Unit**
Height UMR	2,37	mm
Diameter UMR	1,5	mm
Surface area UMR	13,95	mm^2
Volume UMR	0,89	mm^3
Volume Magnet	1,005	mm^3
Mass Magnet	8	mg

3 Conclusions

The trials for the 1.5 mm UMR have shown to be successful, which implies that the UMR can be deployed for medical procedures. The cerebral vasculature is a region difficult to reach and this factor only increases as the diameter decreases. Having modern solutions to reach this tortuous network could potentially lead to a decrease in invasiveness and recovery time. Conditions such as strokes and aneurysms that occur in this system can be treated more efficiently, which could lead to a reduction in severity and improved quality of life for patients. The navigation within the cerebral vascular phantom has been precise and an ideal frequency range to perform the control in has been determined. Challenges such as surpassing bifurcations, overcoming steep pathways and navigating through varying diameters have been successfully overcome and shows that the UMR can be used in a variety of trajectories. Additionally, the UMR was able to reach an aneurysm which could be an effective medical procedure to induce coagulation and therefore treat the aneurysm.
Using the 1.5 mm UMR should result in exploration of the entire cerebral vasculature and will provide a minimally invasive solution to the current procedures. These trials should be performed in a viscous fluid mimicking blood and flow should be added, to ensure real life circumstances.

References

[1] L.-J. W. Ligtenberg, M. C. J. de Boer, I. Mulder, R. Lomme, D. Wasserberg, E. A. M. K. Rot, D. B. Ami, U. Sadeh, H. R. Liefers, O. Shoseyov, P. Jonkheijm, M. Warlé, and I. S. M. Khalil, "X-ray-guided magnetic fields for wireless control of untethered magnetic robots in cerebral vascular phantoms," 2024.

[2] D. Roland, B. Quentin, L. Sean, G. P, L. Jonas, C. Christophe, G. Simone, B. Jatta, S. Dominic, O. K. Nicole, R. Michael, W. Miriam, R. Luca, and N. Bradley, "Dexterous helical magnetic robot for improved endovascular access," *Science Robotics*, 2024.

[3] J. Leclerc, H. Zhao, D. Bao, and A. T. Becker, "In vitro design investigation of a rotating helical magnetic swimmer for combined 3-d navigation and blood clot removal," *IEEE Transactions on Robotics*, 2020.

[4] E. N. Marieb and K. Hoehn, *Human Anatomy Physiology*, 12th ed. Pearson, 2023.

[5] M. Junjie Zhao, H. Lin, R. Summers, M. Mingmin Yang, P. Brian G. Cousins, and M. Jan-

ice Tsui, "Current treatment strategies for intracranial aneurysms: An overview," 2018.

[6] R. Seller, "Complications of interventional treatment of cerebral aneurysms," *Interventional Neuroradiology*, 2008.

[7] M. C. J. de Boer, L.-J. W. Ligtenberg, I. Mulder, C. Goulas, A. Klingner, R. Lomme, E. A. K. Rot, D. Wasserberg, Y. Lu, R. Liefers, J. K. van der Mijle Meijer, G. J. M. Tuijthof, D. B. Ami, U. Sadeh, O. Shoseyov, J. Leclerc, A. T. Becker, P. Jonkheijm, M. Warlé, and I. S. M. Khalil, "Wireless mechanical and hybrid thrombus fragmentation of ex vivo endovascular thrombosis model in the iliac artery," 2024.

[8] RoboDK Inc., "Robodk: Robotic simulation software," 2025. [Online]. Available: https://www.robodk.com

[9] The MathWorks, Inc., *MATLAB Documentation: [Coefficient of Determination (R-squared)]*, accessed: 24-12-2024. [Online]. Available: https://nl.mathworks.com/help/stats/coefficient-of-determination-r-squared.html

[10] D. Chicco, M. J. Warrens, and G. Jurman, "The coefficient of determination r-squared is more informative than smape, mae, mape, mse, and rmse in regression analysis evaluation," *PeerJ Computer Science*, pp. 3–4, 2021.

[11] K. G and J. P., "Guiding hmsc adhesion and differentiation on supported lipid bilayers," *Adv Healthc Mater*, 2016.

[12] L.-J. W. Ligtenberg, F. R. Halfwerk, N. C. A. Rabou, C. Goulas, W. C. Duinmeijer, J. Arens, R. Lomme, V. Magdanz, A. Klingner, E. A. M. K. Rot, C. H. E. Nijland, D. Wasserberg, H.RemcoLiefers, P. Jonkheijm, A. Susarrey-Arce, M. Warlé, and I. S. M. Khalil, "Ex vivo validation of magnetically actuated intravascular untethered robots in a clinical setting," 2024.

[13] R. W. Fox, A. T. McDonald, P. J. Pritchard, and J. W. Mitchell, *Fluid Mechanics*, 9th ed. Wiley, 2016.

[14] D. Brown, "Tracker video analysis and modeling tool," open Source Physics Project. [Online]. Available: https://physlets.org/tracker/